An entropy based multi-thresholding method for semi-automatic segmentation of liver tumors

Anirudh Choudhary[1] Nicola Moretto[2]
Francesca Pizzorni Ferrarese[2] and Giulia A. Zamboni[3]

July 7, 2008

[1]Department of Electrical Engineering, Indian Institute of Technology Kharagpur, India
[2]Altair Lab, Department of Computer Science, University of Verona, Italy
[3]Department of Radiology, University of Verona, Italy

Abstract

Liver cancer is the fifth most commonly diagnosed cancer and the third most common cause of death from cancer worldwide. A precise analysis of the lesions would help in the staging of the tumor and in the evaluation of the possible applicable therapies. In this paper we present the workflow we have developed for the semi-automatic segmentation of liver tumors in the data sets provided for the MICCAI Liver Tumor Segmentation contest. Since we wanted to develop a system that could be as automatic as possible and to follow the segmentation process in every single step starting from the image loading to the lesion extraction, we decided to subdivide the workflow in two main steps: first we focus on the segmentation of the liver and once we have extracted the organ structure we segment the lesions applying an adaptive multi-thresholding system.

Contents

In the Introduction we analyze the problem of segmenting the liver lesions from the clinical point of view. Then we overview the state-of-the-art in the field of liver tumor segmentation. In Section 2 we describe the complete workflow from the analysis of the dataset to the final extraction of the lesions. In the Results part (Section 3) we present the results obtained and in Section 4 we discuss the future improvements we would like to apply to our approach to further optimize the results obtained so far.

1 Introduction

In 2008, an estimated 21,370 adults (15,190 men and 6,180 women) in the United States will be diagnosed with primary liver cancer. An estimated 18,410 deaths (12,570 men and 5,840 women) from the disease will occur this year. Liver cancer is the fifth most common cause of cancer death among men, and ninth most common cause of cancer death among women [12]. The five-year relative survival rate (percentage of patients who survive at least five years after the cancer is detected, excluding those who die from other diseases) of patients with liver cancer is 11%. Unlike many other forms of cancer, the number of people who develop and die from liver cancer is increasing. Liver cancer is much more common in developing countries within Africa and East Asia. In some countries, it is the most common cancer type and it is predicted that for 2030 it will enter the top 20 causes of death [6]. The liver is the second most commonly involved organ by metastatic disease, after the lymph nodes. In Europe and the United States, a focal liver lesion is more likely to represent a metastatic deposit than a primary malignancy. The true prevalence of metastatic liver disease is unknown because most figures are based on autopsy series that reflect the end stage of a disease process. However, depending on the site of the primary tumor 30-70% of patients dying of cancer have liver metastases.

Prognosis for liver cancer is poor so incidence and mortality patterns are very similar. In order to improve the curability of liver cancer, early detection and accurate staging are critical. Staging is a way of describing a cancer, such as where it is located, if or where it has spread, and if it is affecting the functions of other organs in the body. Doctors use diagnostic tests to determine the cancer stage, and CT scans are widely accepted as the gold standard for liver tumor detection. Knowing the stage helps the doctor decide what kind of treatment is best suited and can help predict a patient's prognosis (chance of recovery). Moreover a proper estimation of the tumor size is useful for several applications such as evaluating the effect of therapies on tumor and changing the treatment plans. Although the largest tumor diameter is widely used as an indication of the lesion size, because of 3D shape of the tumor it may not reflect a proper assessment of this tumor attributes [8]. The tumor volume, on the other hand, suggests an appropriate representation of the tumor size.

One way to find an estimation of tumor volume is to use segmentation algorithms. Even if many research groups have developed different approaches for liver segmentation and volume construction in the last few years, only few have proposed systems for the segmentation of the hepatic lesions. Seo and Chung [10] have developed a method that involves the segmentation and binarization of the hepatic structure, the creation of the image based bounding box and the segmentation of the convex deficiencies. Large convex deficiencies are selected by pixel area estimation, they are then transformed to gray-level deficiencies and finally the boundary tumor is selected by evaluating their variance. As stated by the authors, this approach is only applicable to homogeneous boundary tumors. Besides Seo in [9] worked up the previous approach to segment all the hepatic lesions: after the segmentation of the liver, the optimal threshold is calculated by composite hypotheses and minimum total probability error. Finally, hepatic tumors are segmented using the optimal threshold value. Promising results are shown, even if the approach produce diverse false positives, especially for small tumors. Massoptier and Casciaro [5] first segment the liver by adopting a statistical model-based approach and then apply a wavelet analysis for classifying the tumors. The method proposed reaches good results in terms of sensitivity and specificity, even if it doesn't take into account lesions that show pixel intensity values similar to the vessels. In fact primary and secondary liver tumors show different attenuation values in the different contrast-enhancement phases, therefore their conspicuity to the normal liver will change according to the phase that is analyzed. Most primary tumors and many secondary tumors are hyperdense to the normal liver parenchyma (i.e. hypervascular) in the arterial phase, whereas nearly all malignant lesions (both primary and secondary) are hypodense in the portal and in the delayed phase.

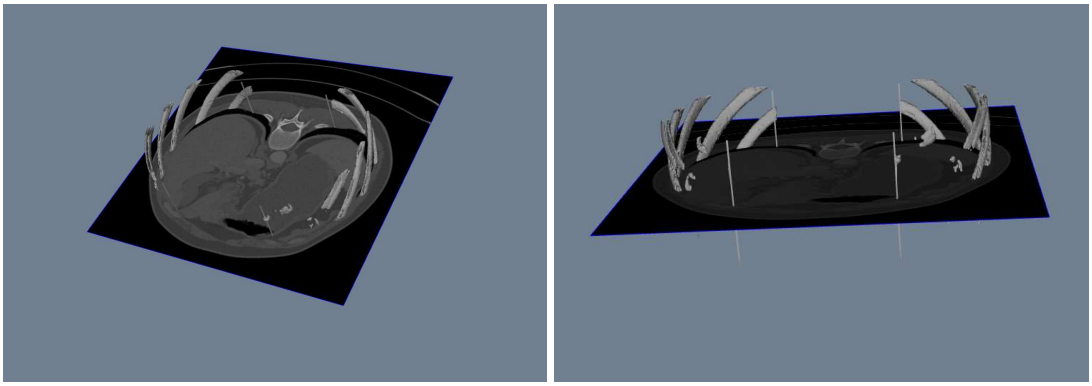

Figure 1: Segmentation of the ribs

2 Materials and Methods

To develop a system which could be as automatic as possible, we decided to proceed sequentially starting from the liver segmentation followed by the lesions segmentation. Our workflow is mainly divided into 2 steps:

- Segmentation of the liver using the ribs and diaphragm constraints.
- Segmentation of the tumor from the segmented liver using multi-thresholding approach.

2.1 Segmentation of the liver

Segmentation of the ribs

With a simple thresholding method we extract the bones, then we subdivide the skeleton in three parts from the axial view and take into account only the first third on the left side, in order to consider only those parts of the ribs that surround the liver. In Fig 1 the extraction and volumetric reconstruction of the ribs is shown. After obtaining the ribs data for different slices we apply a curve interpolation slice by slice using Cubic-Hermite shape preserving interpolation. Since the ribs data is clustered, the mean point for each ribs cluster in a slice is used for the interpolation. All the voxels in the external part of these resulting boundaries are set to 0.

Segmentation of the diaphragm

One of the main problems in liver segmentation is the close proximity between the liver itself and the heart. These two tissues have almost the same density and using region growing methods usually results in the heart being classified as part of the liver. To try to automatize our algorithm as much as possible, we implemented a procedure to identify the diaphragm so that it could be used to constrain the region where the algorithm look for the liver. This idea has already been used in [2], but we implemented a different approach which is computationally more efficient. We have defined this approach since our focus is not in segmenting the liver accurately but in finding the region where it is located, which will then be used as starting point for our tumor segmentation module. The first step toward our goal is to segment the lungs which is an easy task since they are full of air whose Hounsfield value is known. We can then construct a map of the diaphragm

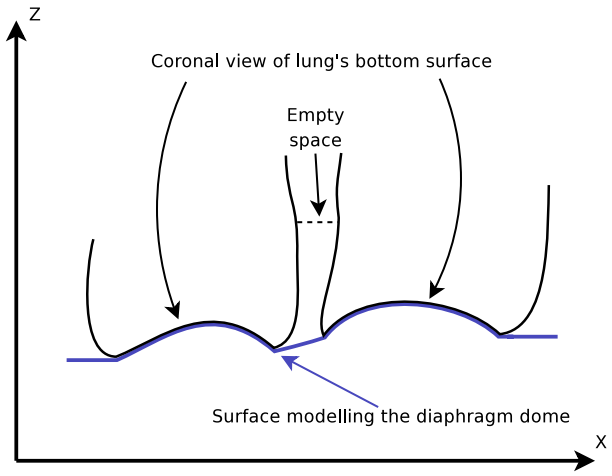

Figure 2: Representation of a section of the lungs surface seen in the coronal plane

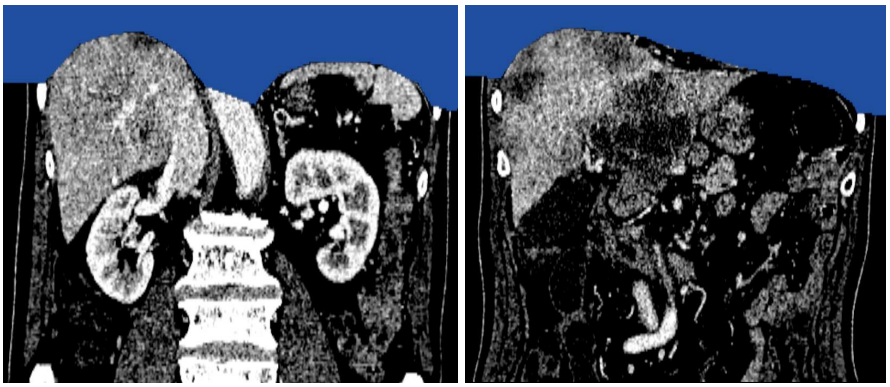

Figure 3: Diaphragm dome approximation

simply considering an axial plane whose dimensions are the same as those of the CT-scan, and assigning to each pixel of the plane the minimum value of the z-axis in the corresponding lung region. This result in an approximation which is wrong in the central part, where the lungs walls are almost vertical. To obtain the correct results, we must interpolate lungs surfaces so that they will be correctly closed (see Fig.2).

To do this we consider the curves obtained sectioning the surface with the coronal plane; each one of them will have an empty space around the center (where the esophagus is placed) which we identify and, starting from the center of this space, we look in both directions until we find the two points of the lungs surface where the slope reaches a threshold. By connecting these two points, we obtain an approximation of the diaphragm for this section. After this procedure is repeated for all slices, we obtain a very good approximation of the entire diaphragm dome, and then all the voxels which are above it are set to 0 (In Fig. 3 these parts are highlighed in blue).

Extraction of liver contours

Since the focus of our work consists in the extraction of hepatic lesions, we only need to identify approximate liver boundaries. In our approach, first of all, we require that the user identifies a slice where the liver appears as the biggest organ or, in cases where it is not possible (i.e. when there are very large tumors), he selects

a point inside the organ. With this initialization, the algorithm, as described in Fig. 4, starts. The algorithm computes the gradient magnitude of the image and then it processes the results to highlight boundaries and normalize image intensities.

We apply the watershed segmentation algorithm that has been introduced in [13] and then used and extended in many fields. Watershed has two parameters that must be specified, the threshold value (below which everything is set to 0 in the input image) and the minimum height of the basins. Both parameters need to be selected to limit the oversegmentation that watershed usually creates.

If the user has previously identified a point inside the liver, we consider the class containing that point as the one representing the liver. If a point has not been selected, classes are ordered by their area and we consider the first one having mean and variance values (computed using original image values) compatible with that of the liver.

Given this first slice of the liver, we estimate its mean ($\bar{\mu}$) and variance ($\bar{\sigma}$), so as to calibrate our system on the specific dataset being studied, and the system starts a sequence of post-processing tasks in order to obtain a mask to be used in subsequent steps. This post-processing includes level-set smoothing and dilation of the region. The resulting region of interest (ROI) will then be used in the next slice as a binary mask such that, after the magnitude gradient and the watershed have been computed, only classes inside the mask will be considered. For each class i, mean (μ_i) and variance (σ_i) are estimated and if the conditions in (1) are satisfied, the class is considered as part of the liver.

$$\|\mu_i - \bar{\mu}\| < \frac{3}{2}\bar{\sigma} \quad \text{and} \quad |\sigma_i - \bar{\sigma}| \leq \bar{\sigma}/2 \tag{1}$$

In (1) we compare both the mean value and the variance, since in the proximity of the liver there could be many structures whose mean values are close to the one of the liver, but the texture may differ. Hence, comparing the σ gives us a hint to distinguish them. A more precise method that we are investigating consists in using textures modelling to better discriminate liver from other organs, as in [7].

This process is repeated for each slice and ends when the area of the liver becomes too small (i.e. below 25 pixels for standard images with resolution 512x512)

Since the process doesn't start from a particular slice, after the last slice has been reached it is necessary to repeat it again from the starting slice in the other direction. At the end, using all the slices a 3D model of the liver is obtained. In Fig 5 all the aforementioned steps are shown for the liver of dataset 5.

2.2 Segmentation of the tumors

Using the liver data obtained, a Haar Wavelet based de-noising algorithm is used for removing the noise from the liver images. Then a minimum cross-entropy multi- thresholding algorithm segments out the tumors. In order to smoothen the final results the system applies morphological closing and 3D level sets to the bidimensional contours obtained. In the next paragraphs these processing steps are described more in detail.

2D segmentation using wavelet based de-noising followed by multi-thresholding

The first step is applying wavelet based de-noising to reduce the high frequency noise in the liver images. For de-noising, a Haar wavelet transform is computed from the original image: the number of scales of decomposition depends on the amount of noise present in the image. Noise level at each wavelet scale is

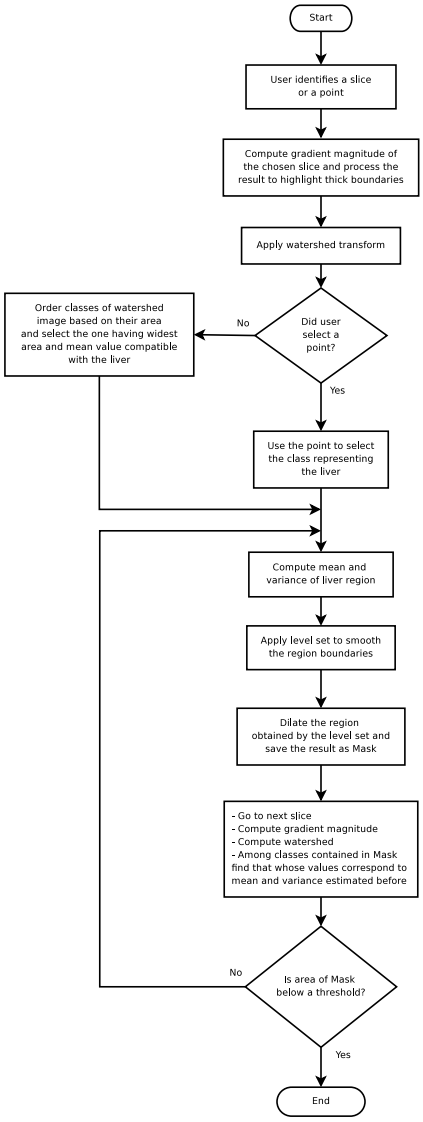

Figure 4: Flowchart of liver segmentation technique

estimated separately and eliminated using soft thresholding. The computation of the thresholds for horizontal, vertical and diagonal coefficient matrices at different wavelet scales is done using the BayesShrink thresholding technique. Then an inverse wavelet transform is applied on the coefficient matrices generating the de-noised image with the tumor region being more uniform as compared to the tumor in noisy image (Fig. 7 a,b).

On the de-noised liver images, a cross-entropy minimization based multi-thresholding technique [4] is applied slice by slice to segment out the tumor. De-noising is necessary before thresholding otherwise the system would segment the tumor along with other regions (mostly noise) connected to it as shown in Fig. 7 c,d. The cross entropy was first proposed by Kullback in [3]. The cross entropy D between 2 probability distributions $F = f_1, f_2, \ldots, f_N$ and $G = g_1, g_2, \ldots, , g_N$ is an information theoretic distance defined by

$$D(F,G) = \sum_{i=1}^{N} f_i \log \frac{f_i}{g_i} \tag{2}$$

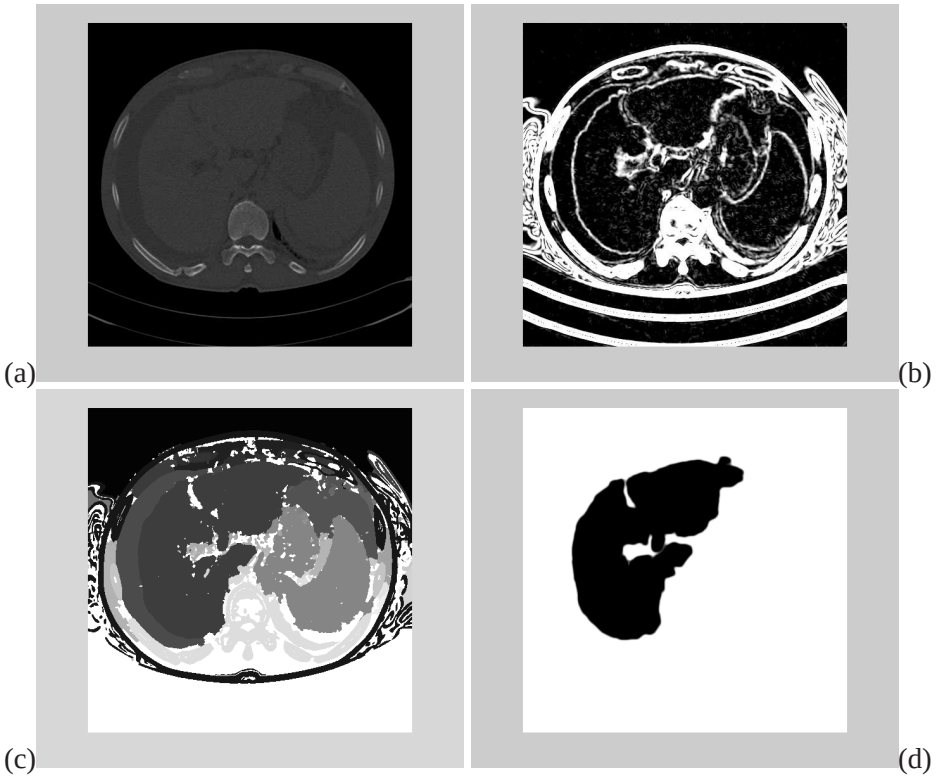

Figure 5: Watershed segmentation step on dataset 5: (a) original image (slice 140), (b) gradient image, (c) result of the watershed segmentation and (d) computed liver mask

The aforementioned approach selects the thresholds by minimizing the relative entropy between the original image and its thresholded version. Let I be an image with $h(i), i = 1,2,...n$ as the corresponding histogram with n being the number of gray levels. The minimum cross entropy thresholding tries to calculate the thresholds ($t_1, t_2 and t_3$) by minimizing the cross entropy, given by

$$D(t_1,t_2,t_3) = \sum_{j=0}^{4} \sum_{i=t_j}^{t_{j+1}-1} ih(i) \log\left(\frac{i}{\mu(t_j,t_{j+1})}\right),\ t_0 = 1,\ t_4 = n+1 \tag{3}$$

where

$$\mu(a,b) = \sum_{i=a}^{b-1} ih(i) / \sum_{i=a}^{b-1} h(i) \tag{4}$$

The number of thresholds applied in each slice is 3 and within a particular slice the dark (i.e. hypodense) tumors lie below the first threshold while the bright (i.e. hyperdense) tumors lie above the third threshold. While moving from a normal liver slice to a slice which contains the tumor, there is a sufficient amount of shift in the first threshold but while moving among slices containing the tumor the first threshold value almost remains the same. This criterion is used for differentiating the pathological slices from the normal ones and estimating a global threshold below which the tumors in these slices lie. The bright tumors are always segmented as white regions lying above the third threshold. The 3D regions obtained after thresholding constitute the dark and the bright tumors as well as other tissues having the intensity similar as the tumors. The second stage involves segmentation of the tumor of interest taking an input point from the user.

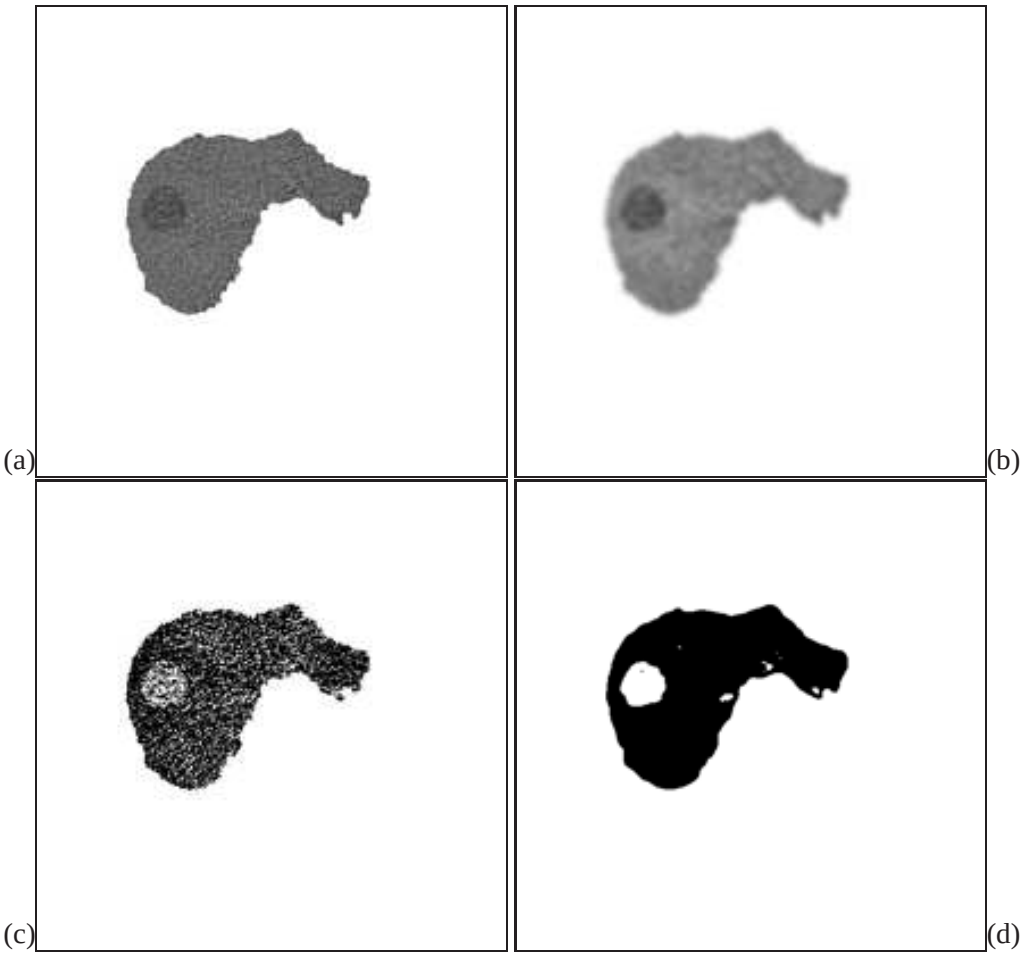

Figure 6: (a) Original image, (b) de-noised image, (c) thresholding applied on the original image and (d) thresholding applied on the de-noised image

Segmentation refinement of the thresholded tumors

For each segmented 3D region, mean (μ) and variance (σ) are computed. A 3D neighbourhood connected region growing is then initiated from the centre of that region taking the lower threshold limit as ($\mu - 6\sigma$) and upper threshold limit as ($\mu + 2\sigma$). This method refines the boundary of all the regions segmented and also segments the complete tumor in those datasets in which the liver region excludes the lesion as we discuss in Section 3. The next step is to eliminate the noise attached to the segmented regions using slice connectivity criteria. Starting from the first slice of each region, we correct the segmentation error by eliminating the artifacts attached to the regions using the fact that the contours in adjacent slices must be similar. While moving among slices we expand and smoothen the boundary of the region in the current slice using 2D level sets and considering only that part of the region in the next slice which lies within this boundary. The bi-dimensional region contours obtained are subjected to morphological dilation and closing to fill the holes and obtain smoother 2D contours. After this step we obtain different 3D structures that have to be classified in order to distinguish between tumors and other elements, e.g. vessels or non-filtered noise. For this purpose the system applies shape constraints. For each structure, a singular value decomposition is estimated and the eigenvalues $\{\lambda_i\}_{i=1..3}$ obtained are analyzed applying the following rules:

- if the λs have almost the same values, the structure is spherical. Evaluate its mean Hounsfield value:

if its lower than the average pixel intensity of the liver, classify it as a tumor;

- if two λs are very big with respect to the third one, then let it unclassified;
- if one λ has a very large value compared to the other two and the Hounsfield value is higher than the average pixel intensity of the liver, classify it as a vessel;
- leave all the other regions as unclassified.

Surface smoothening using 3D Level sets

To further improve on smoothness, 3D Min/Max flow is applied to the segmented tumor [11]. Min/Max Flow is a kind of level set method based on the partial differential equation

$$I_t = -F_{min/max}|\nabla I| \tag{5}$$

where I_t is the temporal derivative of the time-varying image function, ∇ the spatial gradient, $F_{min/max}$ the propagation speed. The latter is calculated as

$$F_{min/max} = \begin{cases} max(-\kappa, 0) & \text{if } average_\kappa(x,y) < 0 \\ min(-\kappa, 0) & \text{otherwise} \end{cases} \tag{6}$$

Here κ is the curvature, $average_\kappa$ the average intensity value within radius κ around a point (x,y). For 3D case we compute κ as follows:

$$\kappa_{3D} = \frac{(I_{yy}+I_{zz})I_x^2 + (I_{xx}+I_{yy})I_z^2 + (I_{xx}+I_{zz})I_y^2 - 2I_xI_yI_{xy} - 2I_xI_zI_{xz} - 2I_yI_zI_{yz}}{(I_x^2+I_y^2+I_z^2)^{3/2}} \tag{7}$$

Examples of the smooth surface of the tumor after applying Min/Max flow are demonstrated in Fig. 7.

At the end, all the unclassified regions, as well as the tumors, are highlighted to the user who can click on those he recognizes to be of interest.

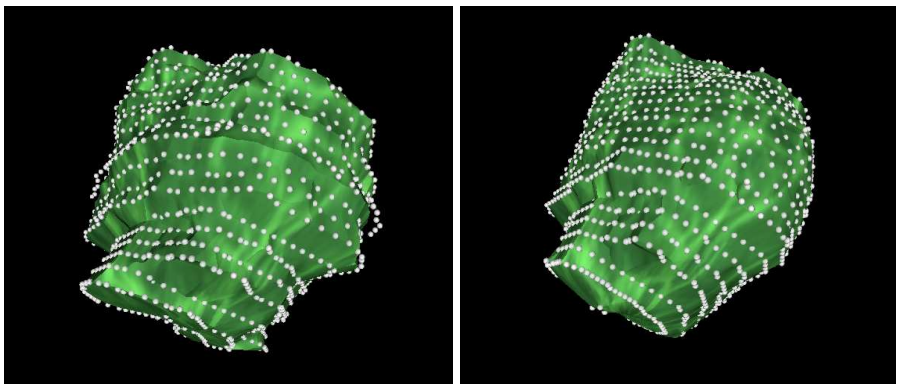

Figure 7: Results of the 3D level set smoothening step on tumor L2 of dataset 7

Table 1: Results of the comparison metrics and scores for all ten test tumors

	Overlap Error		Volume Diff.		Avg. Surf. Dist.		RMS Surf. Dist.		Max. Surf. Dist.		
Tumor	(%)	Score	(%)	Score	(mm)	Score	(mm)	Score	(mm)	Score	Tot.
IMG05_L1	35.10	73	19.69	80	2.74	31	3.79	47	12.87	68	60
IMG05_L2	29.68	77	25.65	73	1.00	75	1.41	80	6.03	85	78
IMG05_L3	43.66	66	35.66	63	1.86	53	2.63	63	7.68	81	65
IMG06_L1	30.34	77	9.52	90	0.77	81	1.03	86	4.23	89	84
IMG06_L2	35.27	73	28.10	71	0.77	80	1.09	85	5.21	87	79
IMG07_L1	23.88	82	2.87	97	3.07	23	4.27	40	18.69	53	59
IMG07_L2	30.47	76	5.88	94	1.56	60	2.10	71	9.10	77	76
IMG08_L1	17.85	86	11.61	88	1.99	50	2.76	61	11.72	71	71
IMG09_L1	45.65	65	78.18	19	2.11	47	2.60	64	9.74	76	54
IMG10_L1	29.53	77	8.61	91	1.78	55	2.27	68	7.64	81	75
Average	32.14	75	22.58	77	1.77	56	2.40	67	9.29	77	70

3 Results

Our method has been applied to 10 CT datasets of oncological patients. Some functions are implemented using the Insight Toolkit [1]. For the gradient magnitude filter, σ value of 1.7 was found to work perfectly for all the cases. For the watershed segmentation, the level and threshold parameters depended on the protocol used to acquire the data. A higher threshold value resulted in a smooth liver boundary but it also led to the disappearance of weaker edges between the liver and the nearby organs in images with poor resolution. A lower level value resulted in oversegmentation of the liver because of the high amount of noise present inside the organ. However, for most of the cases the optimal threshold value for watershed segmentation was determined to be 0.1 after contrast enhancement of the gradient magnitude image. For de-noising the number of decomposition levels was either 2 or 3 depending on the extent of noise present in the image and the non-homogeneity of the tumor regions (e.g. for dataset 5 this value was set to 3 and for dataset 6 it was set to 2). The system evaluates the segmentation accuracy by comparing the segmentation results with the manual segmentation done by experienced radiologists. This system has been successfully applied to the data sets provided for the contest, with a final score of 70. As evident from the Table 1, the accuracy was greater in case of uniform and smaller tumors while for bigger one the accuracy was lower mainly due to greater non-uniformity in their intensities. There were some problems with the watershed segmentation of the liver in datasets in which the tumor occupied a major part of the organ, like dataset 10 (Fig 8) and hence the tumor was left out. But since we have some slices of the liver containing the lesion, so by initiating 3D region growing from any of these tumor slices obtained after thresholding, we can segment out the complete tumor from the dataset. Therefore, we decided to apply 3D region growing as a post processing step to refine the segmentation of the tumor in all datasets.

4 Discussion and Future Work

In this work we have developed a complete workflow aimed at the semi-automatic segmentation of hepatic lesions. After the extraction of the organ boundaries by applying watershed segmentation, the system extracts both the dark and bright tumors using minimum cross entropy multi-thresholding. The results obtained show the effective efficiency of our approach. Besides, while evaluating our algorithm on data sets other than the ones provided for the contest, we have faced problems for segmenting tumors completely lying on the boundary in some particular clinical protocols. Moreover, since traditional multi-thresholding

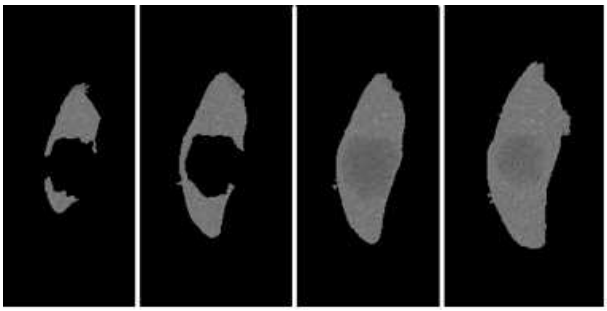

Figure 8: Results of the watershed segmentation in dataset 10

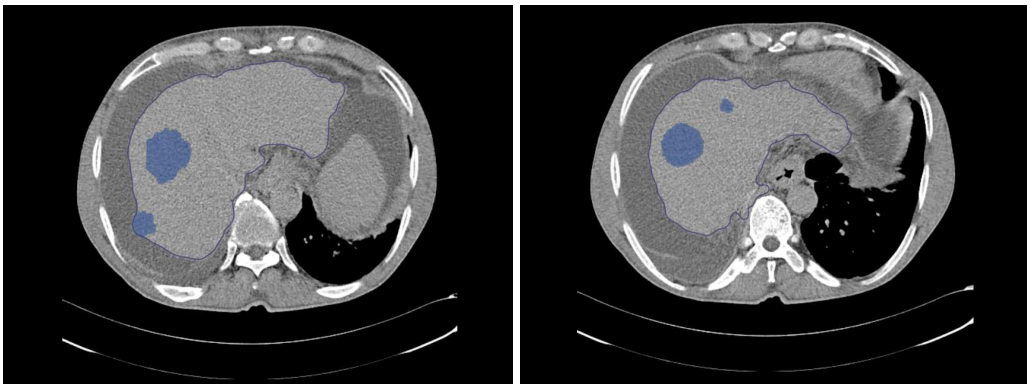

Figure 9: Final results of the complete workflow for dataset 7: the liver is segmented (blue line) and the lesions are highlighted (blue regions)

techniques could be computationally expensive, we want to optimize our system using genetic algorithms. We are currently investigating the possible application of our approach to other abdominal structures, such as the pancreas.

5 Acnowledgments

The work described in this paper has been partially funded by the European Commission's Sixth Framework Programme under contract no. 045201 as part of the Specific Targeted Research Project AccuRobAs (Accurate Robotic Assistant).

References

[1] Insight Toolkit. Available at: http://www.itk.org. 3

[2] R. Beichel, G. Gotschuli, E. Sorantin, et al. Diaphragm dome surface segmentation in ct data sets : A 3d active appearance model approach. *Progress in biomedical optics and imaging*, 3(1):475–484, 2002. 2.1

[3] S. Kullback. *Information Theory and Statistics*. Dover Publications, 1968. 2.2

[4] C.H. Li and C. K. Lee. Minimum cross entropy thresholding. *Pattern Recognition*, 26(4):617–625, 1993. 2.2

[5] L. Massoptier and S. Casciaro. A new fully automatic and robust algorithm for fast segmentation of liver tissue and tumors from ct scans. *Eur Radiol*, 2008. 1

[6] World Health Organization. World health statistics 2008. Technical report, WHO Press, 2008. 1

[7] M. Pham, R. Susomboon, T. Disney, D. Raicu, and J. Furst. A comparison of texture models for automatic liver segmentation. In *Medical Imaging 2007: Image Processing. Edited by Pluim, Josien P. W.; Reinhardt, Joseph M.. Proceedings of the SPIE, Volume 6512, pp. 65124E (2007).*, March 2007. 2.1

[8] S. Saini. Radiologic measurement of tumor size in clinical trials: past, present, and future. *American Journal of Roentgenol*, 176(2):333–334, 2001. 1

[9] K.S. Seo. Automatic hepatic tumor segmentation using composite hypotheses. In *ICIAR*, pages 922–929, 2005. 1

[10] K.S. Seo and T.W. Chung. *Computational Science and Its Applications – ICCSA 2005*, volume 3483/2005, chapter Automatic Boundary Tumor Segmentation of a Liver, pages 836–842. Springer Berlin / Heidelberg, 2005. 1

[11] J. Sethian. *Level Set Methods and Fast Marching Methods: Evolving Interfaces in Computational Geometry, Fluid Mechanics, Computer Vision, and Materials Science*. Cambridge University Press, 1999. 2.2

[12] American Cancer Society. Cancer facts & figures 2008. Technical report, Atlanta: American Cancer Society, 2008. 1

[13] L. Vincent and P. Soille. Watersheds in digital spaces: An efficient algorithm based on immersion simulations. *IEEE Transactions on Pattern Analysis and Machine Intelligence*, 13(6):583–598, 1991. 2.1